Supporting information

Symmetry breaking in gold-silica-gold multilayer nanoshells

Ying Hu,[†] Sterling J. Noelck,[†] and Rebekah A. Drezek [†,]*

[†] Department of Bioengineering, Rice University, Houston, TX 77005, [*]Department of Electrical and Computer Engineering, Rice University, Houston, TX 77005.

Corresponding email: drezek@rice.edu

Surface charge distributions from circularly polarized light

The charge distribution on multilayer nanoshells (MNS) is more complex when incident light is circularly polarized. We demonstrate in Figure S1 the surface charge plots that correspond to the case where incident light is composed of two equal components in the axial (y) and transverse (x) direction and are 90° out of phase. One can observe that the charge distribution for the octupole and quadrupole resonance shares some similarities with the distribution in the axial case; whereas the dipole distribution is similar to the transverse case. The major observations, however, are consistent with the hybridization analysis. For instance, the inner and outer gold surfaces possess the same charge

polarization, indicating the bonding nature of the shell mode interacting with the core mode. The opposite charge polarization on the inner core surface reveals the bonding nature of the hybridized mode.
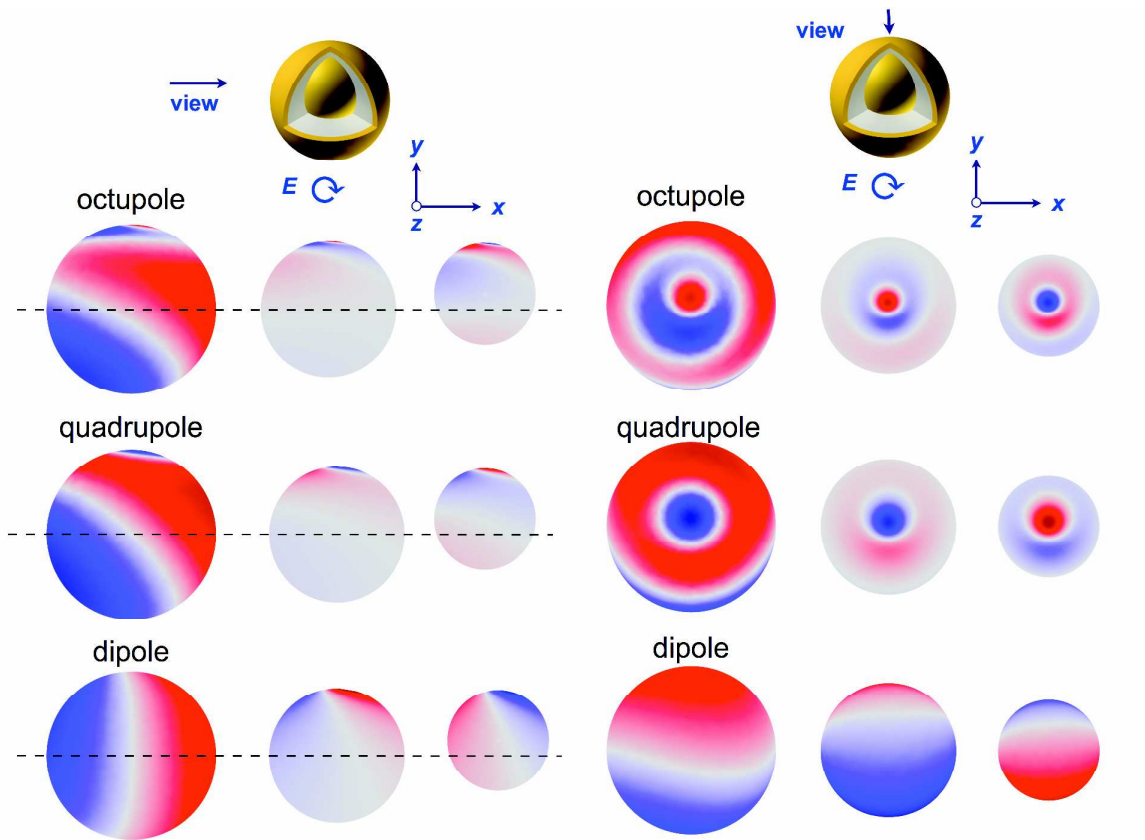

Figure S1. Side (left) and top (right) views of the surface charge plot of R30/40/50 nm MNS with 9 nm core offset at various hybridized plasmon peaks as the incident light is circularly polarized. The circular polarization is in the *x-y* plane, the offset is in *y* and the wave propagates in *z*. The three columns correspond to the outer gold shell (left), inner gold shell (middle), and inner gold core (right) surfaces. Red: positive charges, blue: negative charges. Horizontal dashed lines in the left panel mark the center location and show the core offset.

Absorption relative to scattering

In the R20/30/50 nm MNS case, both the dipole and quadrupolar extinction peaks have larger scattering components than in the concentric geometry. However, as the core offsets, the dipole scattering component starts to decrease almost immediately and fall below the absorption component for a core offset of 6nm, shown in Figure S2a. While the R20/30/50 nm MNS appears to scatter more strongly than R30/40/50 nm MNS, the trend of an increasing absorption relative to scattering still holds for larger core offsets.

The quadrupolar peak is more complicated as it is not fully separated from the anti-bonding mode until the offset is larger than 6 nm. The anti-bonding peak is composed of a mixture of modes that could account for the higher absorption values for the 6 nm extinction peak. At larger offsets, as Figure S2b demonstrates, the scattering component initially increases and then decreases while the absorption continuously increases. The overall scattering-to-absorption trend still resembles what was seen in the R30/40/50 nm MNS case although for this particle the scattering peak is dominant.
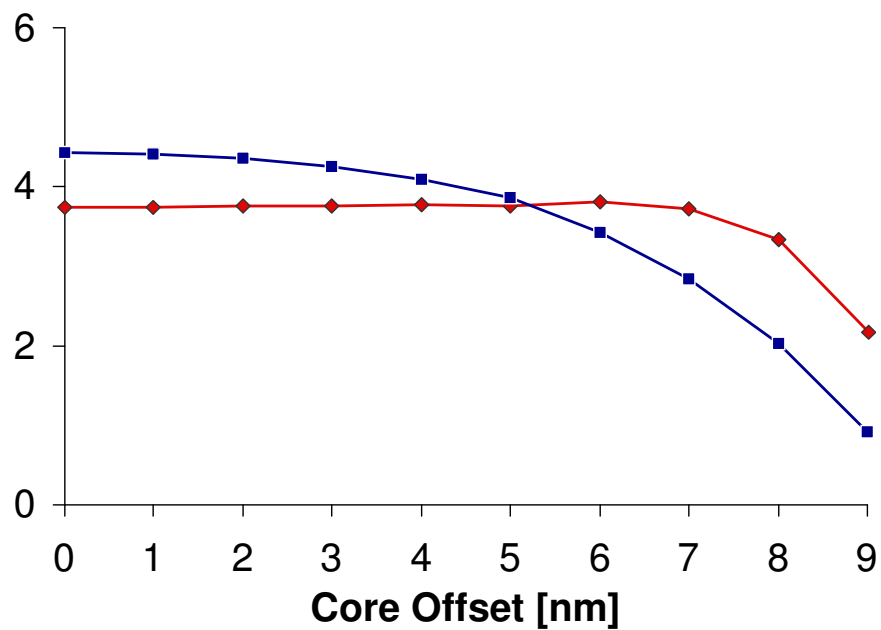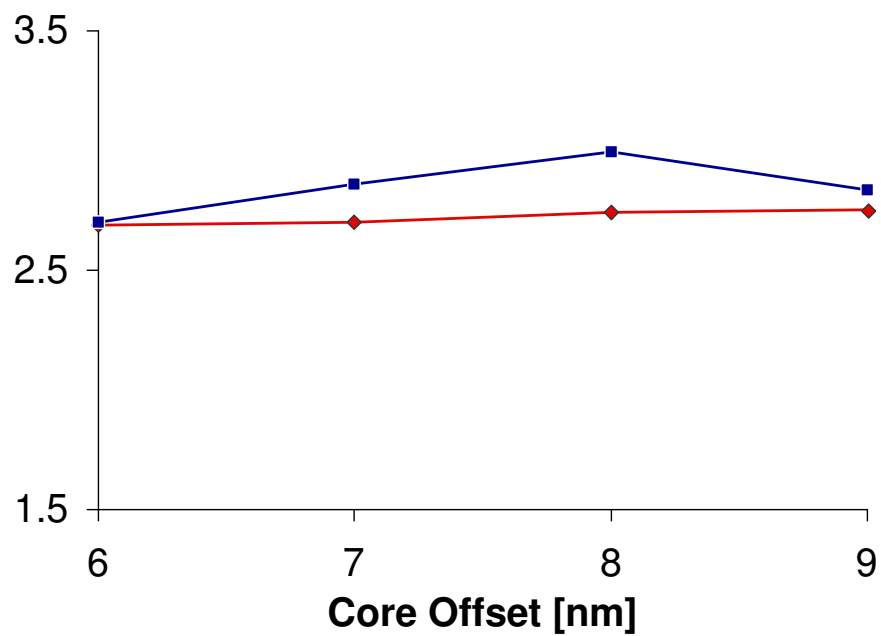
Figure S2. FEM calculations of the absorption (red) and scattering (blue) efficiency of the R20/30/50 nm MNS with a variable core offset in water at the dipolar resonance (a) and the quadrupolar resonance (b). The incident light was transversely polarized.